Interfaces: Adsorption, Reactions, Films, Forces, Measurement Techniques, Charge Transfer, Electrochemistry, Electrocatalysis, Energy Production and Storage

Interactions between mutant bacterial lipopolysaccharide (LPS-Ra) surface layers: Surface vesicles, membrane fusion, and effect of Ca and temperature

Christian Redeker, and Wuge H Briscoe

Langmuir, **Just Accepted Manuscript** • DOI: 10.1021/acs.langmuir.9b02609 • Publication Date (Web): 11 Oct 2019

Interactions between mutant bacterial lipopolysaccharide (LPS-Ra) surface layers: *Surface vesicles, membrane fusion, and effect of Ca^{2+} and temperature*

Christian Redeker[$], Wuge H. Briscoe*

School of Chemistry, University of Bristol, Cantock's Close, Bristol, BS8 1TS, UK

[$] Present address: Abitz & Partner mbB, Arabellastr. 17, D-81925 München, Germany

*Corresponding author; E-mail: wuge.briscoe@bristol.ac.uk; Tel: +44 (0)117 3318256

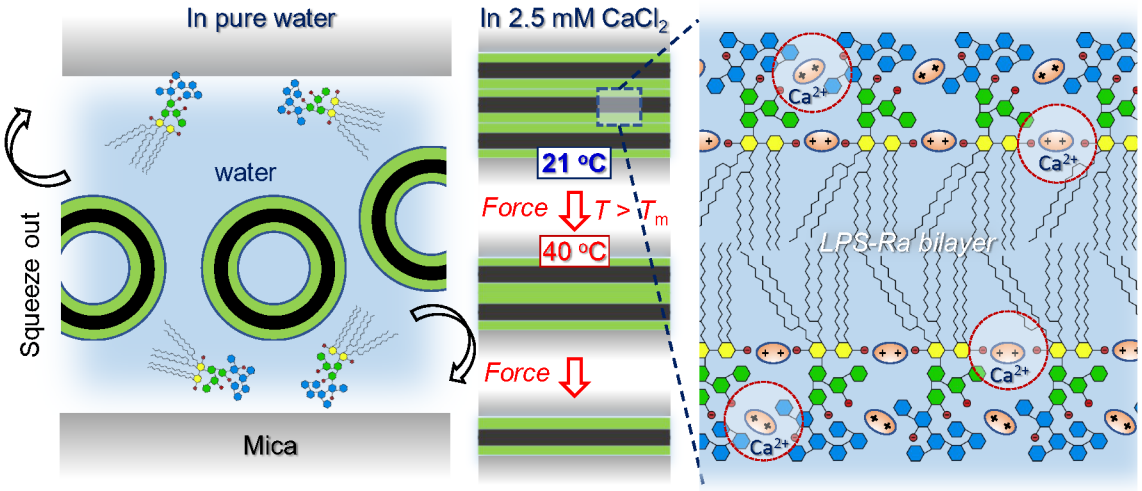

Abstract

Lipopolysaccharides (LPS) are a major component of the protective outer membrane of Gram-negative bacteria. Understanding how the solution conditions may affect LPS-containing membranes is important to optimising the design of antibacterial agents (ABAs) which exploit electrostatic and hydrophobic interactions to disrupt the bacteria membrane. Here, interactions between surface layers of LPS (Ra mutants) in aqueous media have been studied using a surface force apparatus (SFA), exploring the effects of temperature and divalent Ca^{2+} cations. Complementary dynamic light scattering (DLS) characterisation suggests that vesicle-like aggregates of diameter ~28-80 nm are formed by LPS-Ra in aqueous media. SFA results show that LPS-Ra vesicle adsorb weakly onto mica in pure water at room temperature (RT), and the surface layers are readily squeezed out as the two surfaces approach each other. However, upon addition of calcium (Ca^{2+}) cations at near physiological concentration (2.5 mM) at RT, LPS multilayers or deformed LPS liposomes on mica are observed, presumably due to bridging between LPS phosphate groups and between LPS phosphates and negatively charged mica mediated by Ca^{2+}, with a hard wall repulsion at surface separation D_0 ~ 30-40 nm. At 40 °C which is above the LPS-Ra β-α acyl chain melting temperature (T_m = 36 °C), fusion events between the surface layers under compression could be observed, evident from δD ~ 8-10 nm steps in the force-distance profiles attributed to LPS-bilayers being squeezed out due to enhanced fluidity of the LPS acyl-chain, with a final hard wall surface separation D_0 ~ 8-10 nm corresponding to the thickness of a single bilayer confined between the surfaces. These unprecedented SFA results reveal intricate structural responses of LPS surface layers

to temperature and Ca^{2+}, with implications to our fundamental understanding of the structures and interactions of bacterial membranes.

Introduction

Antibiotic resistance has become an increasingly important issue due to excessive use of antibiotics in agriculture and health industry[1-3], whilst development of new antibiotics has become stagnated. The bacterial cell wall can be a target for effective and alternative antibacterial agents due to its accessibility and its significance in cell communication, protection and regulation[4-7]. It is thus crucial to study the structure and to understand fundamental interactions at the bacterial cell wall.

Bacteria can be broadly classified into Gram-positive and Gram-negative species according to the staining properties due to their different cell wall structures, which are distinct from those of eukaryotic cells. Both types of bacteria have an inner cytoplasmic phospholipid membrane with a distal layer rich in peptidoglycan, which is significantly thicker in Gram-positive bacteria (30-100 nm). Gram-negative bacteria possess an additional highly asymmetric outer membrane, containing an inner phospholipid and an outer bacteria-specific lipopolysaccharide (LPS) leaflet (Figure 1A), offering an extra polymer brush-like protective coating[4]. Despite a high degree of structural variability, some general features of LPS from different bacteria can be identified. It consists of a conserved hydrophobic anchor, lipid A, and a polysaccharide head group, which can be further divided into a moderately conserved, short core and a highly

variable, long O-antigen[8]. Mutant LPS with truncated head groups, ranging from free lipid A to a full core (Ra mutant; Figure 1B) have been used as model systems to study the influence of the carbohydrate chain architecture on LPS properties[9, 10].

LPS not only serves as a protective coat, it can also trigger lethal septic shocks when released into bloodstream in a molecular or aggregate form[11, 12]. Therefore, a number of strategies in the combat against bacteria have targeted LPS. For instance, naturally occurring cationic antimicrobial peptides (AMPs) exploit the presence of negatively charged inner core and lipid A of LPS by binding electrostatically and subsequently disrupting the membrane[13-15]. Naturally occurring and synthetic surface adsorbing peptides and polymers have been reported to bind LPS specifically to remove LPS and bacteria from solutions[16-18]. Other studies have reported LPS crosslinking induced by cationic peptides and polymers, which can lead to the suppression of the endotoxic effect[19-21].

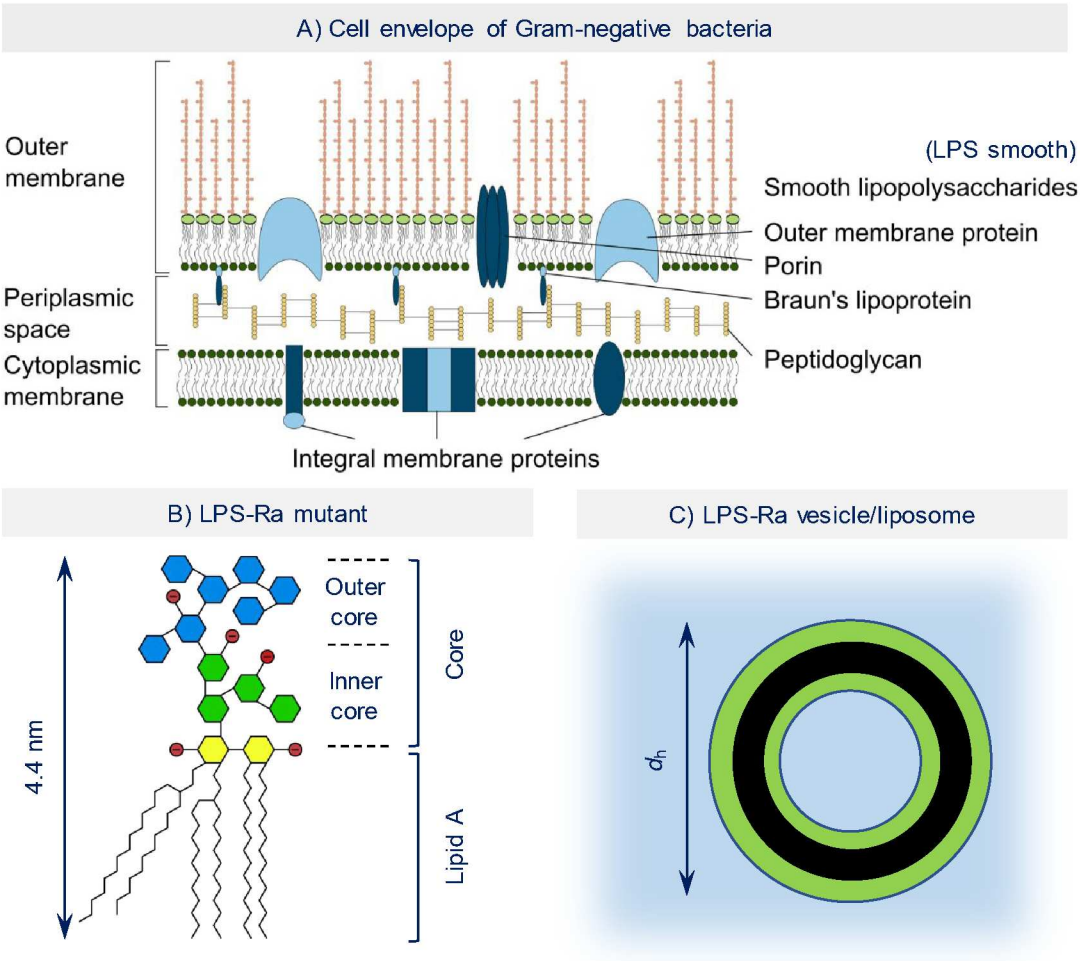

Figure 1. A) Schematic representation of the cell envelope of Gram-negative bacteria, showing the inner (cytoplasmic) and outer membranes and their main constituent molecules (including different proteins and the inter-liking peptidoglycan layer in the periplasmic space). Smooth lipopolysaccharides (LPS) are a major component of the outer leaflet of the outer membrane (Adapted from [22]). B) Schematic showing the structure of LPS-Ra mutant, with lipid A and inner and outer core regions. C) Possible LPS-Ra vesicle structure as suggested by the hydrodynamic diameter d_h from DLS measurement of the LPS-Ra aggregation in aqueous media, with the dark inner region representing LPS tails and the green regions LPS headgroups.

Bacterial model membranes based on natural and mutant LPS have been prepared including monolayers at the air-water interface[23-25] and hydrophobized surfaces[26, 27],

supported symmetric and asymmetric bilayers[9, 28], and multilayers[29]. These model membranes have been used to elucidate structural properties and interactions of immobilised LPS monolayers with abiotic surfaces such as mica as well as polystyrene- and APTES-coated mica[27]. Adsorption behaviour of LPS from aqueous solution on abiotic surfaces has also been studied[30-35]. In addition, the effects of different salts[24], antimicrobial peptides[23], and temperature[29] on these model membranes have been studied experimentally and using computer simulations[36-40].

Generally, LPS adsorption and interactions at surfaces have been considered as being governed by H-bonding[32], hydrophobic forces[34] and electrostatic forces[27, 31, 35]. Despite these studies, there remain considerable gaps in our fundamental knowledge on how physical parameters, such as the LPS carbohydrate chain length and conformation, substrate surface physicochemical properties, and electrolytes, affect the structure of the adsorbed LPS layers and the interactions at the LPS membrane surface. Some consistencies and debates persisted in the literature. For instance, Tong et al.[31] reported the formation of LPS-Rd and Ra bilayers in buffered solution on mica, while Lu *et al.*[27] observed very little adsorption of LPS-Ra on the same surface. In contrast, they found that *smooth LPS* adsorbed on mica and attributed it to hydrogen (H-)bonding between the LPS and the surface; whereas little adsorption of *smooth LPS* on hydrophilic (GeO_2, Fe_2O_3, and Al_2O_3) and hydrophobic (ZnSe) surfaces was observed by Parikh and Chorover [34].

In comparison to monovalent cations, the presence of divalent cations can significantly alter structural and interaction properties of LPS. Divalent cations can accumulate in

the negatively charged LPS core region[9, 24], possibly crosslinking several lipid molecules[41] and inducing LPS multilamellar phases[42]. This can lead to LPS structural rearrangement, and associated membrane compaction can result in increased bilayer integrity[9] and thus reduced penetration by AMPs[23]. Divalent ions have also been shown to promote adsorption of LPS and bacteria[43] on negatively charged surface[30]. They have also shown strong effects on supramolecular aggregation of LPS in solution[10, 44], which has been related to their interfacial adsorption behaviour[34].

In this study using the surface force apparatus (SFA) [45, 46], we have investigated the adsorption behaviour of aggregates of LPS-Ra mutant (Figure 1, with its detailed chemical structure shown in Figure S1 in the Supplementary Information (SI) section) on negatively charge mica, and the interactions between these adsorbed layers; in particular, the effects of temperature and presence of Ca^{2+} have been evaluated. The aggregate size has been characterised using DLS. Our results show that LPS Ra adsorption was significantly increased in the presence of Ca^{2+}. In addition, the stability of the adsorbed layer altered as the temperature was raised above the gel to liquid crystalline (β-α) acyl chain melting temperature of LPS-Ra (T_m = 36 °C)[10].

Experimental

Materials

Lipopolysaccharide (rough strain) from *Escherichia coli* EH100 Ra mutant (Sigma Aldrich®), calcium chloride ($CaCl_2$; Acros Organics, ACS reagent grade) were used.

Ultrapure Milli-Q water (Resistivity: 18.2 MΩ cm, total organic content (ToC) < 4 ppb) was used throughout for the solution preparation.

Preparation and DLS/zeta potential characterisation of LPS-Ra aqueous dispersion

The extrusion method was used to homogenise the LPS-Ra aggregate size, as DLS suggested that highly polydisperse aggregates of size tens of nm – tens of μm existed in the non-extruded LPS-Ra solution. LPS-Ra (0.1 mg mL^{-1}) in ultrapure Milli-Q water or in 2.5 mM aqueous $CaCl_2$ solution was vortexed for 30 sec before extrusion using a 10 mL LIPEX extruder (Thermobarrel, Northern Lipids Inc.) in combination with a temperature controlled water bath (Grant Scientific, Optima T100 + TC120) at a pressure ~ 5 bar. The solution was first extruded six times through two polycarbonate membranes (Whatman Nuclepore Track-Etch polycarbonate membrane, diameter 25 mm) with a pore size of 0.2 μm, and then further six times through two polycarbonate membranes of pore size 0.1 μm, all at 80 °C to obtain a transparent solution. The hydrodynamic diameter (d_h) and zeta potential (ζ) of the resulting solutions were obtained using dynamic light scattering DLS (Nano Zetasizer ZS, Malvern Instruments). Approximately 1 mL of the extruded solutions was injected into a plastic cuvette (Fisher, UV Grade Cuvettes) and the DLS measurements of d_h were taken, with the analysis performed using Zetasizer Software 7.12. Electrophoretic mobility (μ_e) measurement was made using disposable folded capillary cells (Malvern Instruments, DTS1070), with the sample left to equilibrate for at least 2 min prior to the measurement. The obtained μ_e was converted to ζ potential using the approach described by Delgado et al.[47], which has its limitations when the ζ value is greater than

±50 mV[48]. We will have performed comprehensive ζ measurements of LPS mutant aggregates in solutions of monovalent and multivalent ions, which will be discussed in a separate publication (Redeker et al., in preparation).

Atomic force microscopy (AFM) imaging of morphology of surface layers

AFM (Bruker Multimode 8, Peakforce feedback control) was used to image the morphology of LPS-Ra aggregates absorbed on mica. A ~1 cm x 1 cm mica sheet was glued onto an AFM magnetic disk using Epon 1004 (Shell) and subsequently the top layers of mica removed using a piece of sticky tape to expose a clean, molecularly smooth surface. The disk was incubated overnight in approximately 30 mL of extruded LPS (0.1 mg mL^{-1}; equivalent of 24.6 μM) aqueous dispersion (either in MilliQ water or 2.5 mM $CaCl_2$ solution) at 21 °C prepared as described above. The AFM disk was then transferred to the instrument with a drop of the solution on top to ensure continuous wetting of the surface. A liquid cell containing aqueous $CaCl_2$ solution of the same concentration as the sample under investigation was mounted above the surface to prevent the surface from drying out during the measurement. Bruker Scanasyst silicon nitride cantilevers were used for imaging (spring constant 0.7 N m^{-1}, tip radius 2-5 nm). Images were obtained in the tapping and Quantitative NanoMechanical (QNM) mode. Scan rates between 0.2-3 Hz were used with image sizes ranging from 0.1-10 μm. Images were recorded and processed, including flattening to account for sample tilting and low pass filters to smoothen the image, using the Bruker NanoScope Analysis 1.80 software package. To investigate the effect of temperature on the adsorption and morphology of LPS-Ra aggregates on mica

(Islas et al. in preparation), disks were incubated in 30 mL LPS-Ra solution at 45 °C for 1-12 h. Subsequently, the solution containing the disks were left to cool to room temperature and then imaged as described above at room temperature.

Measurements using the Surface force apparatus (SFA)

The SFA [45, 46, 49] was used to obtain normal (F_N) and shear (F_s) forces between two mica surfaces immersed in aqueous LPS dispersions as a function of surface separation (D). Mica (S & J Trading Inc., A1 special grade) was cleaved by hand in a particle-free laminar flow hood (LFH) to 2-7 μm thick sheets, which were then cut into ~1 x 1 cm pieces using a white-hot platinum (Pt) wire (99.9999% pure; Sigma), and immediately laid down on a freshly cleaved mica backing sheet to protect them from dust. Care was taken during the cutting so that the mica sheets "upstream" in the LFH from the Pt wire, so that they were not exposed to any possible nanoparticles generated by the hot wire. A thin layer (~ 40 nm) of silver (Ag beads, Aldrich, purity: 99.9999%) was deposited onto the mica using thermal evaporation under ~ 10^{-6} Torr (Edwards Coating System E306A). The mica sheets were then glued onto cylindrical quartz disks using Epon 1004 (Shell) with the silvered side down, and the disks were mounted in a crossed cylinder configuration.

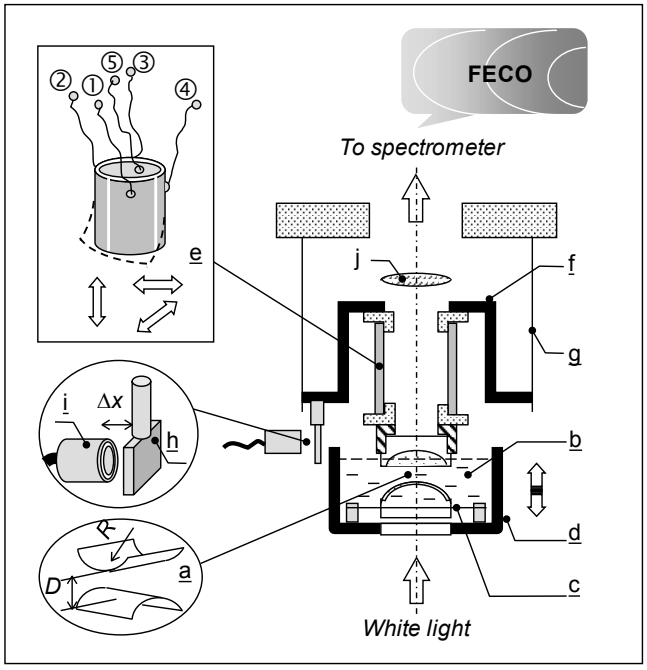

Figure 2. Schematic showing the key components in an SFA. The closest separation *D* between two gently curved mica surfaces (inset a; *R*~ 1 cm) is monitored to ± 0.2 nm using the technique of the fringes of equal chromatic order (FECO). The surfaces can be immersed in an intervening medium (b) housed in a liquid bath (d). The surface force F_N is measured by the deflection of spring (c). Shear motion is facilitated by applying an electrical voltage to a sectored PZT tube (inset e), attached to the vertical spring (g) via a rigid bridge (f), with the spring deflections gauged by an air capacitance (± 0.3 nm) probe (inset h) which gives friction F_s.

As schematically shown in Figure 2, the SFA used in the experiments incorporates the shear measurement capability based on Klein's design (who termed it the Surface Force Balance, SFB)[45, 49], extended and modified to enable the surface separation control and data acquisition using a custom designed digital interface and a modern Shamrock 500i spectrometer coupled with a Neo sCMOS camera (Andor, Oxford Instruments). The top surface is attached to a four-sectored piezoelectric tube, which is mounted on a pair of leaf springs (of spring constant k_s = 120 N m^{-1}), whose deflections are monitored by a capacitance probe (Accumeasure 9000 MT

Instruments) with ~ 1.5 nm resolution. The lower surface is also mounted on a pair of leaf springs (k_N = 100 N m^{-1}) in a liquid cell, which is attached to a linear stepping motor (Physik Instrumente (PI) GmbH & Co. KG) within a motion range of 20 mm, a step size <1 nm, and a speed range between 1 and 10^5 nm s^{-1}. The upper surface can be moved parallel to the lower surface by the application of an oscillatory voltage of designated amplitude and frequency (e.g. a sawtooth function with a peak to peak amplitude of 3 μm) to the piezoelectric tube. Digital signal traffic control and monitoring input and output is managed using a field programmable gate array (FPGA) via a LabView interface programme.

Surface separation D in the SFA is monitored using fringes of chromatic order (FECO) based on multiple beam interferometry in the optical cavity of silvered mica surfaces, by shinning a beam of collimated white light generated by an arc lamp (Newport Spectra-Physics Ltd.). The FECO fringes are resolved in a Shamrock 500 spectrometer with a Neo sCMOS camera at speeds of up to 100 frames per second. Images of FECO during approach and separation of the surfaces are recorded with the time-stamped motor position. The digital FECO spectral images can be converted into surface separations using the transfer matrix method[50]. The force acting between the two surfaces at any given separation D can be calculated as $F_N(D) = k_N \Delta D$ where ΔD is the deflection of the horizontal springs, i.e. $\Delta D = D - D'$ with D' extrapolated from the linear surface separation *vs*. motor position plot at large D where the force is absent. Similarly, the shear force F_s can be determined from the deflection Δx of the shear springs measured with the capacitance probe, i.e. $F_s(D) = k_s \Delta x$.

Approximately 18 mL of the LPS dispersion was injected between the two surfaces in a specific sequence (LPS-Ra in water, LPS-Ra in 2.5 mM aqueous $CaCl_2$ solution and pure water) and normal and shear forces between the surfaces measured in each solution at a temperature below (21 °C) and above (40 °C) the phase transition temperature of LPS Ra (36 °C [10]). The SFA results below represent data collected from 20 different contact spots from 5 separate experiments.

Results and discussion

DLS of LPS-Ra aggregates and AFM imaging of LPS-Ra surface layers

Figure 3A shows that the DLS hydrodynamic diameter d_h of the extruded LPS-Ra dispersion increased from 28 ± 5 nm in pure water to ~70-90 nm in 5-10 mM $CaCl_2$ at room temperature (~21 ^oC), and the corresponding zeta potential ζ became less negative concomitantly. Such a self-association behaviour in solution is largely consistent with previous DLS studies which reported aggregate hydrodynamic diameters ranging from 14-95 nm for different rough and smooth LPS[51-54] and ζ ~-30 mV for LPS-Ra in HEPES buffered solution (pH 7)[55]. Given the molecular length of the LPS-Ra of 4.4 nm (Figure 1B), we postulate that they formed vesicle-like structures in both pure water and the $CaCl_2$ solution (also see AFM images in Figure 4 below). Cryogenic transmission electron microscopy (CryoTEM) has previously revealed a variety of structures of unextruded LPS aggregates[56, 57] ranging from spherical, to fibrillar and toroidal structures depending on the presence of electrolytes and

carbohydrate chain length. In particular, for non-extruded LPS in HEPES buffer, CryoTEM showed vesicular structures for lipid A (diameter range from 100 nm to 3 μm), LPS-Re (diameter range from <100 nm to ~250 nm) and LPS-Rc (diameter range from 250 nm to 500 nm) from Salmonella enterica sv. Minnesota; while non-extruded LPS-Ra in HEPES buffer from the same bacterial species showed predominately ribbon-like bilamellar structures (of greater than some hundred nanometers in length)[56]. These observations of vesicular aggregate formation for LPS mutants are in agreement with our postulated aggregate structure, although Richter et al.[56] showed predominately ribbon-like bilamellar structures for LPS-Ra. Such a discrepancy may be due to different solution conditions (i.e. LPS-Ra concentration and pH value) and the bacterial origin of LPS-Ra used by Richter et al.[56] compared to our study. Furthermore, it is conceivable that the long ribbon-like bilamellar structures of Richter et al.[56] may be transformed into vesicles by the extrusion process. Finally, freezing LPS-Ra vesicles for CryoTEM sample preparation could have also led to the collapse of vesicular LPS-Ra structures into the observed ribbon-like bilamellar structures. It should be acknowledged that It is extremely challenging to characterise the LPS aggregate structures using classic neutron and X-ray scattering methods (which we are currently pursuing) due to the size and structural complexity/diversity. In this study, we have homogenised our samples *via* extrusion to reduce the structural complexity and polydispersity, as required by SFA measurements.

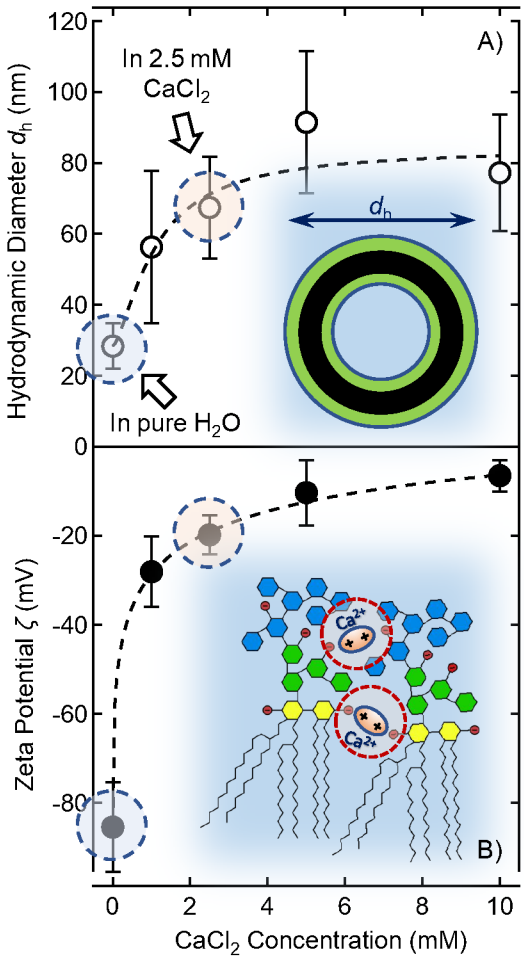

Figure 3. A) Hydrodynamic diameter d_h of LPS-Ra aggregates as a function of $CaCl_2$ concentration at 21 °C, measured using the dynamic light scattering (DLS) method. The inset schematic shows the postulated vesicle aggregate structure. B) Zeta potential ζ *vs.* $CaCl_2$ concentration. The dashed lines are a guide to the eye, and the dark-blue dashed-circles indicate data points in pure water and 2.5 mM $CaCl_2$, respectively, conditions under which SFA measurements have been performed. The inset schematic shows Ca^{2+} bridging (red dashed-circles) between negatively charged phosphate groups in the adjacent lipid A headgroup and inner/outer core regions of Lipid-Ra.

Divalent cations have been reported to accumulate in the negatively charged phosphate groups in the LPS core and the lipid A headgroup region (cf. Figure 3B inset) [9, 24], and the enhanced inter-molecular binding could conceivably enhance the effective membrane rigidity, leading to a decrease in the aggregate curvature and thus

an increase in d_h, as Ca^{2+} concentration increased. The interpretation of increased Ca^{2+} adsorption to LPS-Ra aggregates with the $CaCl_2$ concentration is also consistent the ζ potential data shown in Figure 3B, with ζ decreasing from ~-85 ± 10 mV in pure water to -10 ± 5 mV due to cation adsorption. In contrast, the aggregate d_h values remained largely constant at ~28 nm in 1-10 mM NaCl (data not shown; Redeker et al., ms in preparation). The dark-blue dashed circles in Figure 3 indicate the data points for the solution conditions (pure water and 2.5 mM $CaCl_2$) in which the SFA measurements have been performed, i.e. the aggregate size d_h = 28 ± 5 nm and 68 ± 13 nm and the corresponding zeta potential ζ = -85 ± 10 mV and -20 ± 5 mV in pure water and 2.5 mM $CaCl_2$, respectively.

Figure 4 shows representative AFM height images of mica immersed in the extruded 0.1 mg mL^{-1} LPS-Ra dispersions in water and 2.5 mM $CaCl_2$ at 21 ^oC, with the imaging undertaken after the mica surface was incubated in the dispersion at ~45^oC, above the melting temperature T_m = 36 ^oC of the lipid tails in LPS-Ra, and then cooled down to 21 ^oC. Little adsorption of any LPS-Ra aggregates as observed in water (Figure 4A; corresponding 3D image shown in Figure S2 in SI), with some small (a few nm in the lateral dimension) surface features that could be attributed to small patches of adsorbed LPS-Ra – possibly aggregate fragments, consistent with the surface force curve ② in Figure 5 discussed below. In contrast, 2D height image in Figure 4B and 3D image in Figure 4C show the presence of the adsorbed surface layers in 2.5 mM $CaCl_2$, with the surface layer exhibiting spherical or ellipsoidal shapes of different sizes (~50-250 nm) and heights (50-100 nm, cf. the line profile in Figure 4B). We attribute

the observed surface structures to adsorbed LPS-Ra aggregates, probably with loose distal layer(s) atop an underlayer, and our initial analysis (Islas et al., in preparation) of the lateral size of the surface aggregates is consistent with them deformed/flattened laterally. The morphology (i.e. spherical-like) is also broadly consistent with the DLS d_h results (Figure 3A), substantiating in part the postulation that LPS-Ra vesicles formed in solution. Further experimental evidence, e.g. using small-angle neutron scattering (SANS), could provide corroborating evidence for vesicle formation. However, our preliminary SANS experiment showed weak scattering from the aggregates in in the LPS-Ra concentration range in which these aggregates were stable.

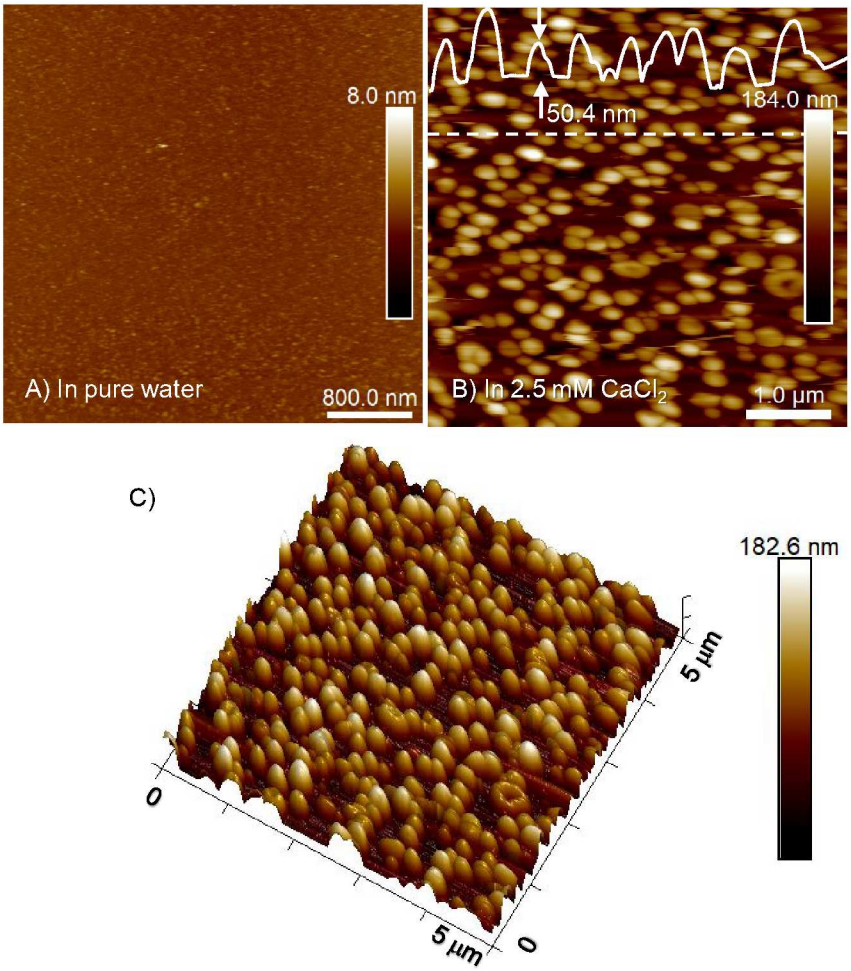

Figure 4. (A) AFM height image (4 µm x 4 µm) of mica immersed in 0.1 mg mL^{-1} LPS-Ra dispersions in pure water, showing little surface adsorption. The corresponding 3D image is shown in Figure S2 in the SI section. (B) AFM height image (5 µm x 5 µm), with the corresponding 3D image (C), of mica immersed in 0.1 mg mL^{-1} LPS-Ra dispersion in 2.5 mM $CaCl_2$, showing adsorbed layers of aggregates. The imaging was undertaken after the surfaces were incubated in the respective dispersion at ~ 45 °C and then cooled down to 21 °C. An example cross section line profile along the white dashed-line in the figure reveals surface aggregates of different heights (50-100 nm, with one of them indicated) and widths (~100-150 nm), attributed to the adsorbed flattened LPS-Ra vesicles, possibly with additional adsorption atop an underlying layer.

Nonetheless, it is clear from Figure 4 that Ca^{2+} has a significant effect on the adsorption behaviour of the extruded LPS-Ra dispersion on mica. In pure water, the repulsion between the negatively charged LPS-Ra core and lipid A headgroup and

negatively charged mica surface sites vacated by desorption of lattice K^+ would suppress any significant LPS-Ra adsorption. In 2.5 mM $CaCl_2$, inter-LPS bridging by Ca^{2+} would have enhanced the stability of the vesicles against spontaneous fusion and bilayer formation on the surface observed with liposomes[58]. Similar trends of increased resistance to rupture upon Ca^{2+} addition have been reported for supported 1.2-dipalmitoyl-*sn*-glycero-3-phosphocholine (DPPC) and DMPC bilayers[59]. Concurrently, divalent Ca^{2+} could bridge the similarly charged lipid A heagroups and mica surface sites (cf. Figure 6), in a manner not unlike the intramolecular bridging effect that Ca^{2+} exhibits between negatively charged LPS-Ra phosphate groups. Enhanced LPS-Ra vesicle stability and augmented LPS-mica binding mediated by Ca^{2+} would have facilitated the observation of the relatively stable surface vesicle layer by AFM imaging in Figure 4B,C. The morphological details of LPS-Ra aggregates adsorbed on mica depended on Ca^{2+} concentration and solution temperature, effects currently under investigation (Redeker et al. ms in preparation).

Interactions between mica surfaces immersed in LPS-Ra dispersions in pure water

Figure 5A shows example profiles (Curve ①) of the normal force normalised by the effective surface radius vs. surface separation (F_N/R vs. D) between two mica surfaces immersed in the extruded LPS-Ra (0.1 mg/mL) dispersions in pure water at 21 °C, both upon approach (empty circles) and retraction (filled circles) between the two surfaces. In pure water, a relatively long-range repulsion (diminishing at ~ D = 60 – 80 nm) was observed, before the surfaces reached a hard-wall repulsion at D_0 = 0 – 3 nm

(which varied from different contact spots). No adhesion was observed upon retraction, with a small hysteresis compared to the approach.

We attribute the observed long-range repulsion – exponential in nature (*cf.* inset to Figure 5A) – to the electrical double layer repulsion arising from the residual surface charge after patchy LPS-Ra adsorption (cf. Figure 4A), which would also account for the short-range repulsion and the hysteresis between the approach and retraction force profiles due to deformation in the patchy layer occurring upon compression and subsequent relaxation upon retraction. The effective decay length of κ^{-1} = ~18-20 nm is much smaller than that in pure water (~96 nm), indicating that LPS-Ra contributed to the background ionic strength and screening. *E. coli* LPS-Ra EH100 carries 3 phosphates, a single phosphoethanolamine (PEtN) and a single pyrophosphoethanolamine (PPEtN) as well as 2 carboxylic groups, thus with a maximum of 11 ionizable groups[60]. Calculation of the Debye length κ^{-1} using the LPS-Ra concentration of 0.1 mg/mL (24.6 μM) and assuming full dissociation of the charged groups and a highly asymmetric (1:11 anion:cation) electrolyte, would yield κ^{-1} = 7.54 nm, much smaller than the fitted decay length. For to obtain κ^{-1} = ~18-20 nm, we would need to assume 3.85-4.34 (or 35-40%) of the 11 groups were charged. Furthermore, aggregation of LPS into different shapes and sizes[56, 57] indicates the presence of an apparent critical aggregation concentration (CAC) which is dependent on the LPS polysaccharide chain length, although no CAC value has been reported for LPS-Ra in the literature. The CAC for short polysaccharide chain mutant LPS-Re and Lipid A from *S. minnesota* were 4 μM and 5 μM respectively[53], although the validity

has been questioned due to experimental limitations[61]. In contrast, Mueller et al.[12, 62] estimated a CAC of ~10 nM for these LPS, while Sasaki et al.[63] found a temperature dependency for LPS-Re: $T < T_m$: 41.2 nM; $T > T_m$: 8.1 nM). The CACs for LPS from heterogenous long O-antigen polysaccharide chain bacterial serotypes ranged from 10 μg/mL to 32 μg/mL[51, 53, 54], depending on the bacterial type. For LPS from *Escherichia coli* serotype 026:B6, a CAC of 14 μg/mL (3.2 μM) was reported in the PBS buffer. For our measurements with LPS in pure water, if only the background (CAC) LPS concentration was used, it would yield a κ^{-1} ~20-30 nm, compared to the fitted value of κ^{-1} = 18-20 nm. Hence, it appears that the charged aggregates and their dissociated counterions might have contributed to the screening in the measured electric double layer force.

A short-range repulsion onset at D ~ 3-5 nm (F_N/R ~40 mN m^{-1}), then increased sharply as the surfaces were pushed closer into contact, attributed to adsorbed LPS on the surface. This hard wall contact separation, D_0 ~ 0-2.8 nm, varied between different contact spots and different experiments, indicating inhomogeneous surface coverage. In the particular force Curve ① shown in Figure 5, there is also evidence of the surface layer being squeezed out from D ~ 1.2 nm to D ~ 0.2 nm, as indicated by the slight discontinuity in the force profile. If we assume symmetric surface adsorption, a surface layer thickness of t ~ 0.6-2.5 nm formed but the distribution was not uniform. At other contact spots, the surfaces could be push to D_0 ~ 0 nm contact, and also there was a slight hysteresis in the force profile as the surfaces were separated (filled circles in the figure). This suggests that at these spots the adsorbed layer could be completely

removed or there was little adsorption - the surface coverage was patchy due to weak adsorption of LPS-Ra (or its vesicle fragments) on the surface. This is likely due to strong electrostatic repulsion between negatively charged mica and LPS-Ra in solution as indicated by a measured zeta potential ζ = -56.7 mV at 25°C for LPS-Ra dispersion in pure water (cf. Figure 3B). The surface layer thickness is also comparable to that detected from SFA experiments by Lu et al.[27], who used a similar LPS-Ra mutant but from a different strain of *Escherichia coli* (K12) in 0.1 M NaCl solution on mica, observing the formation of surface layers of t ~ 1 nm in thickness. In contrast to our results, they found a small adhesion force (-0.7 mN m^{-1}) upon retraction. However, overall the presence of a high concentration of potassium cations seemed to have little effect on the LPS adsorption behaviour.

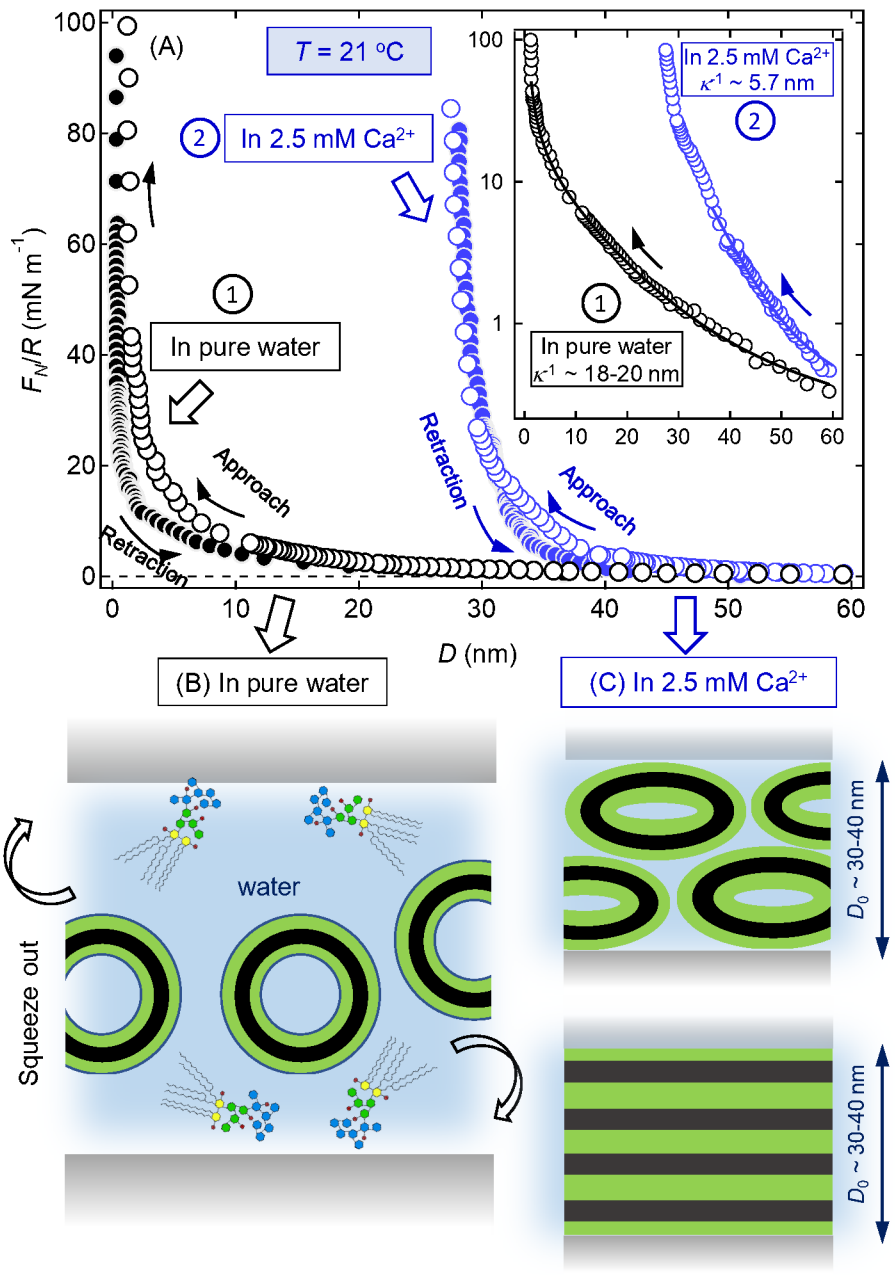

Figure 5. (A) Normal surface force normalised by the contact radius vs. surface separation (F_N vs. D) between mica immersed in 0.1 mg mL^{-1} LPS-Ra dispersions in pure water (Curve ①) and 2.5 mM $CaCl_2$ (Curve ②) at 21 °C upon approach (empty circles) and retraction (filled circles) of the surfaces. The inset shows the corresponding log-linear plot for the approach force profiles, with the solid curves showing the exponential fit to the long-range decay of the force profiles, with the effective Debye length also given (κ^{-1} = 18-20 nm in water and κ^{-1} = 5.7 nm in 2.5 mM $CaCl_2$, respectively). (B) Schematic showing LPS-Ra vesicles being squeezed out in pure water. (C) Schematic showing two possible surface structures giving rise to the surface force profile ② in 2.5 mM $CaCl_2$: surface-

adsorbed flattened LPS-Ra vesicles (top) and multilayers of LPS-Ra membranes due to rupturing of vesicles on the surface. The bridging role of Ca^{2+} is further illustrated in Figure 6.

The surface force profiles were not significantly affected by increased incubation time (up to 1 day) of the surfaces in the LPS solution. Furthermore, increasing the temperature in pure water to above the LPS-Ra β-α acyl chain melting temperature (T_m = 36 °C) had little effect on the surface force profiles, except for a small increase (δt < 1 nm) in the surface layer thickness. This could be attributed to slightly increased adsorption because of reduced electrostatic repulsion due to screening, consistent with a slight decrease in absolute zeta potential value of LPS-Ra dispersion in pure water from ζ = -56.7 mV at 25°C to ζ = –52.5 mV at 40 °C.

Interactions in LPS-Ra dispersions in 2.5 mM $CaCl_2$ at 21 °C (below the melting temperature T_m = 36 °C of LPS-Ra acyl chains)

The addition of 2.5 mM $CaCl_2$ had a dramatic effect on the adsorption behaviour of LPS-Ra on mica. F_N/R vs. D profiles labelled ② in Figure 5A shows example surface force curves between two mica surfaces immersed in the extruded LPS-Ra (0.1 mg/mL) dispersion in 2.5 mM $CaCl_2$ at 21 °C after overnight incubation, upon approach (empty circles) and retraction (filled circles) between the two surfaces. A purely repulsive force was observed when the surfaces were brought into contact. However, the hard wall thickness increased to D_0 = 30-40 nm in 2.5 mM $CaCl_2$ compared to D_0 = 0-2.8 nm in pure water (Curve ① in Figure 5A). Given the LPS-Ra bilayer thickness δD ~ 8-10 nm, D_0 = 30-40 nm could be accounted for by ~ 4 LPS-Ra bilayers, either due to a layer of flattened LPS-Ra vesicles on each surface or due to trapped 4

bilayers from compression-induced vesicle rupture (Figure 5C). These two scenarios could not be distinguished unequivocally from the force profiles at 21 °C, and it is likely that both could occur. However, as we discuss below, our experimental observations point to trapped multilayers between the surfaces under elevated temperatures ($T > T_m$). There is a slight hysteresis in the force profile upon retraction, attributed to the relaxation of the compressed surface layer. The details of the surface profiles varied at contact spots, and another example of the F_N/R vs. D profiles is shown in Figure 6A below (Curve ①) with a more noticeable hysteresis upon retraction. However, the overall consistent feature of the surface force profiles in 2.5 mM $CaCl_2$ is a purely repulsive interaction, reaching a hard wall at D_0 = 30-40 nm.

Preceding to reaching the hard wall, a short-range repulsion with an apparent exponential decay length of κ^{-1} = 5-6 nm was observed (cf. Figure 5A inset; Curve ②). The calculated Debye length in 2.5 mM $CaCl_2$ (overwhelming the LPS-Ra concentration of 24.6 μM) is κ^{-1} = 3.5 nm. An effective background $CaCl_2$ concentration of 1 mM would have been needed to yield κ^{-1} = 5-6 nm, and adsorption of Ca^{2+} could not have been sufficient to account for the depletion of Ca^{2+} concentration. One possibility is that the presence of LPS-Ra might have suppressed dissociation of $CaCl_2$. Alternatively, the repulsion is not solely of an electrical double layer origin; instead, it could be due to elastic deformation of the surface adsorbed LPS-Ra layers, or that of a loosely adsorbed top layer (either vesicles or their fragments) atop the surface layer. We are currently developing an analytic model to possibly relate this short-range repulsion to the elastic modulus of the surface adsorbed layer. However,

the overriding feature of our observation here is the dramatic effect of Ca^{2+} on the adsorption of LPS-Ra layers on mica.

Ca^{2+} is known to bind to the negatively charged phosphate groups in the LPS core and the lipid A headgroup region [9, 24], which is also consistent with our zeta potential data (cf. Figure 3B). Lanne et al. [64] have suggested that phosphate groups may also be present in the outer core of LPS (cf. Figure 1B), and thus Ca^{2+} could also bind to LPS-Ra outer cores. Accordingly, in the schematic of Figure 6 (and also the inset in Figure 3B), the bridging effect of Ca^{2+} between LPS-Ra is shown to be mediated between the negatively charged lipid A headgroups and between the inner and outer cores of LPS-Ra. Furthermore, the enhanced adsorption of LPS-Ra aggregates in 2.5 mM $CaCl_2$ – evident from both the AFM imaging (Figure 4B,C) and the surface force profiles (Curve ② in Figure 5A) – can be attributed to the bridging effect mediated by Ca^{2+} between the negatively charged phosphate groups in the outer and inner cores of LPS-Ra and the negatively charged mica sites residual from desorption of K^+ from the lattice.

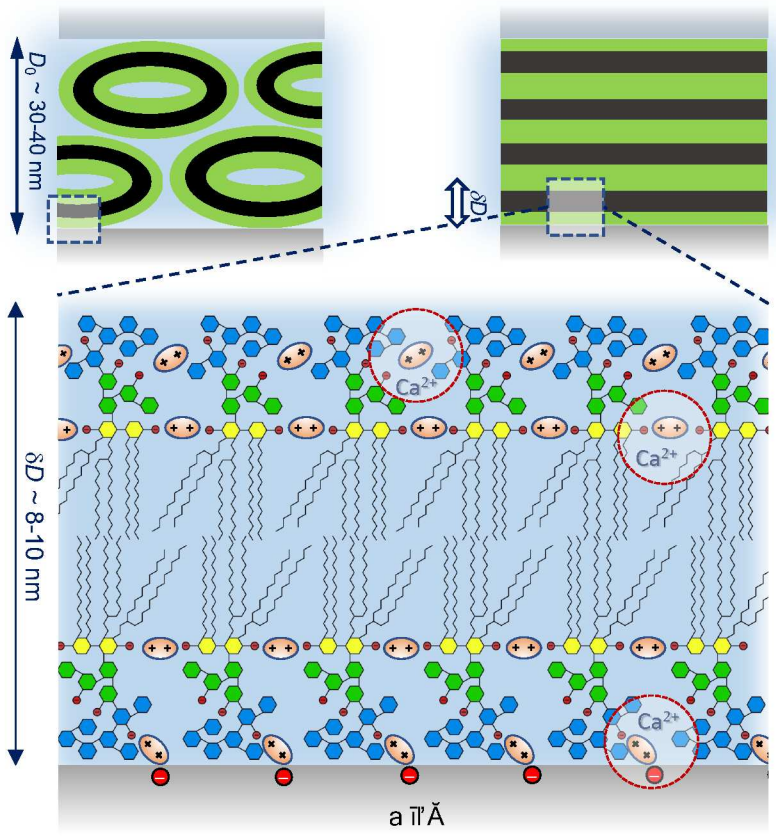

Figure 6. Schematic showing an LPS-Ra bilayer of thickness δD ~ 8-10 nm adjacent to negatively charged mica in $CaCl_2$ solution, applicable to the both scenarios of LPS-Ra vesicles or multilayers at the mica surface. The bridging effect of Ca^{2+} is schematically shown between the negatively charged phosphate groups in the inner and outer core regions of LPS-Ra, and between the negatively charged outer core and the negatively charged mica sites.

Interactions in LPS-Ra dispersions in 2.5 mM $CaCl_2$ at 40 °C ($T > T_m$)

The effect of temperature on the LPS-Ra surface layers was investigated by SFA measurements at temperatures above the β-α acyl chain melting temperature of LPS-Ra (T_m = 36 °C). At 21 °C (Curve ① in Figure 7A), a hard wall was reached at D_0 = 30-40 nm under a compressive force F_N/R up to 700-800 mN m^{-1} (also see Figure 5A). In contrast at 40 °C, an example force profile in Figure 7A (Curve ②; contact spot 1) shows that the surfaces encountered the first hard wall at $D_{0,1}$ = 27 nm, before an

inward step of size δD ~ 9 nm at F_N/R ~ 200 mN m^{-1} to a second hard wall contact $D_{0,2}$ = 18 nm. We attribute the observed force profiles at 40 °C to arising from 3-4 LPS-Ra bilayers confined between the surfaces. The force profile ② on a log-linear scale in the inset in Figure 7A reveals a repulsion preceding the hard wall contact at $D_{0,1}$, which could be attributed to the removal of the loosely attached top LPS-Ra top layer.

As AFM images in Figure 4B,C revealed surface vesicles of LPS-Ra would have formed on a single mica surface. As the surfaces were brought close to each other, the confinement would encourage vesicle rupture to form bilayers, a process further promoted by the enhanced acyl tail fluidity at $T > T_m$. Spontaneous rupture of liposomes or vesicles is a classic method for lipid bilayer formation, which would often lead to single bilayers on a solid substrate (e.g. [58]). The LPS-Ra lipids, with their quite unique molecular architecture, would sustain structural integrity of the vesicles, resisting surface rupture and forming layers of surface vesicles as observed from AFM imaging (cf. Figure 4B,C). The fact that more than 3-4 bilayers were observed between the surfaces points to confinement induced rupture, which would have left the bilayers trapped between the surfaces. As the confined bilayers were further compressed (Figure 7A Curve ②), an LPS-Ra bilayer was squeezed out with a step size δD ~ 9 nm corresponding to the thickness of an LPS-Ra bilayer (as shown schematically in Figure 7B), again facilitated by the enhanced acyl tail fluidity, in a process analogous to the membrane fusion processed first observed by Horn between phospholipid bilayers [65]. The second hard wall contact $D_{0,2}$ = 18 nm indicates that a single LPS-Ra

bilayer remained between the surfaces at the highest compression force at this contact spot.

The force profiles varied somewhat at different contact spots in 2.5 mM $CaCl_2$ at 40 ^oC, with different onset surface separations for the pre-hard wall repulsion and the number of steps (i.e. the number of the bilayers being squeezed out) in the fusion process, suggesting some inhomogeneities in the surface coverage of the adsorbed LPS-Ra vesicles, also consistent with AFM images (cf. Figure 4B,C). Meanwhile, the step size in the force profiles was very similar at different contact spots, i.e. δD = 8-10 nm was consistent throughout, corresponding to thickness of an LPS-Ra bilayer. F_N/R vs. D profile at a different contact spot (Curve ③; main figure in Figure 7 and inset). In this case, the minimum absolute hard wall surface separation was D_0 ~ 10.0 nm at a compression force of up to F_N/R = 1,000 mN m^{-1}, indicating the firm attachment of an LPS-Ra layer between the surfaces, which could not be squeezed out. Prior to the ultimate hard wall, up to 4 steps in the force profiles were observed (**a – d** demarcated by vertical dot-dashed lines; more distinct on the log-linear plot in the inset). The first step (**a**) was initiated at F_N/R ~ 3-4 mN m^{-1} at D = 46.5 nm with a step size δD = 18-19 nm, which could

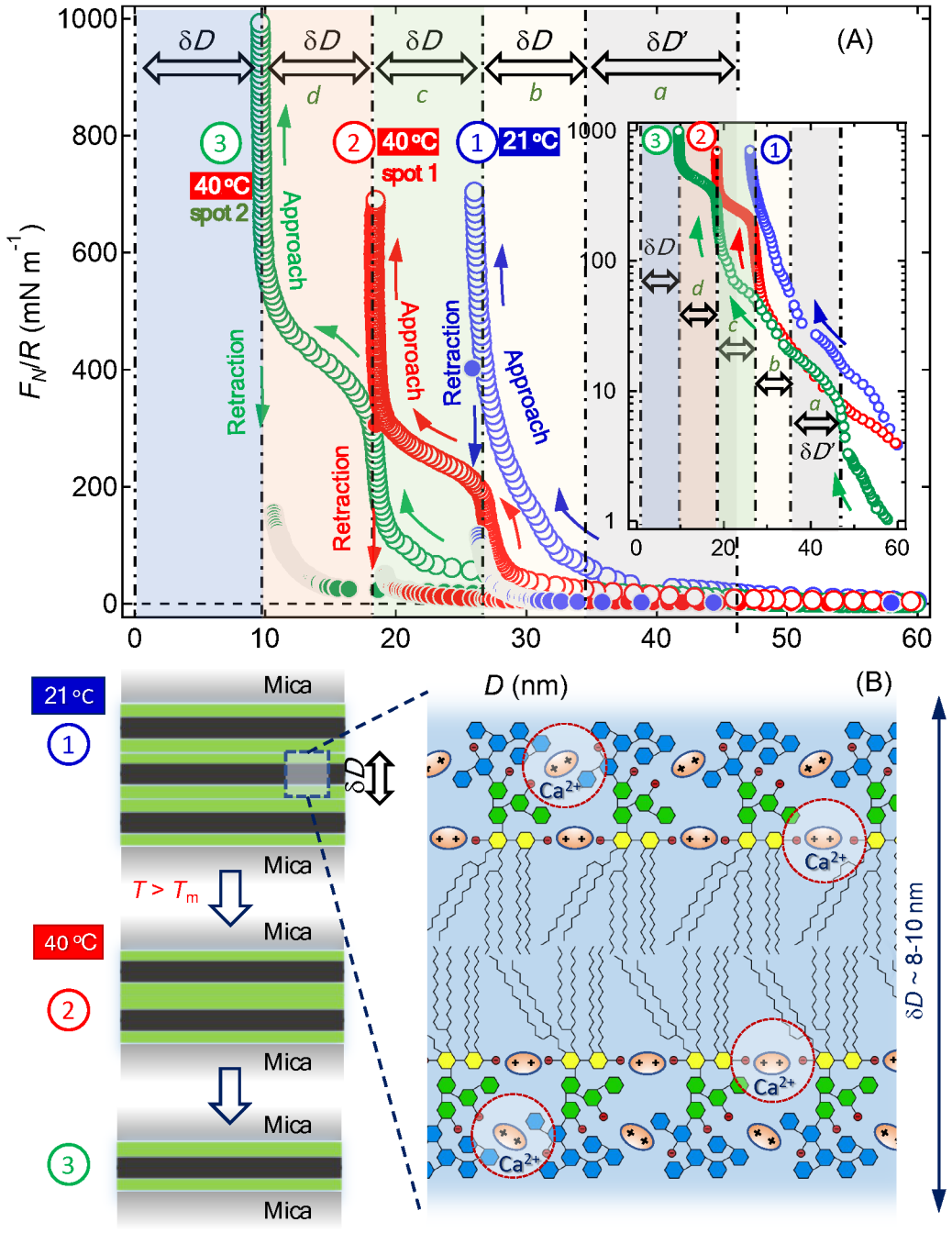

Figure 7. (A) Comparison of the normal surface force normalised by the contact radius vs. surface separation (F_N vs. D) between mica immersed in 0.1 mg mL^{-1} LPS-Ra dispersions in 2.5 mM $CaCl_2$ at **21 °C** (Curve ①) and **40 °C** (at two different contact spots; Curve ② and ③) upon approach (empty circles) and retraction (filled circles) of the surfaces. The inset shows the corresponding log-linear plot for the approach force profiles. As demarcated by the vertical dot-dashed lines, the discrete steps of step size δD or $\delta D'$ are evident in the force profiles at 40 °C (> melting temperature T_m = 36 °C of the acyl chain of LPS-Ra). Labels **a-b** indicate the four steps in Curve ③. (B) Schematic showing 3 LPS-Ra

bilayers being trapped between two mica surfaces (shaded grey rectangles as labelled) at 21 °C, and the hard wall contact at 40 °C after bilayers of LPS-Ra are squeezed out due to the enhanced fluidity of LPS-Ra acyl tails. The schematic on the righthand side of (B) shows an LPS-Ra bilayer with a thickness of δD = 8-10 nm, with the bridging role of Ca^{2+} between phosphate groups in the core and lipid A regions also highlighted.

be due to compression or removal of a loosely attached top layer or vesicle fragments. This was followed by two not-as-well-defined steps (**b** and **c**) onsetting at D = 28 nm and D = 18.5 nm, respectively, with a step size of δD = 9.5 nm, before a well-defined step (**d**) was initated at $F_N/R \sim 350$ mN m^{-1} between D = 18.5 nm and D = 10.5 nm (δD = 8.0 nm). This is consistent with progressive squeeze-out of LPS-Ra bilayers before the final more complete bilayer was squeezed out in the fusion process.

Rinsing the system with water did not alter the force profiles significantly, further underlining the high stability of the LPS-Ra surface layer in the presence of Ca^{2+}. Interestingly, the effect of temperature on the behaviour of the LPS-Ra surface layer was largely reversible, when several heating-cooling cycles were carried out successively.

Our SFA results indicate the presence of 3-4 stacked LPS-Ra layers of thickness δD = 8-10 nm between the surfaces, with possible further loosely bound layers of LPS-Ra aggregate fragments atop. Both the minimum hard wall surface separation D_0 and δD correlate well with the thickness of a LPS-Ra bilayer as determined from using crystallography data (i.e. the length of a single LPS-Ra molecule ~ 4.4 nm)[66]. Temperature dependent fusion of supported 1,2-dimyristoyl-*sn*-glycero-3-

phosphocholine (DMPC) bilayers has been previously observed with SFA – i.e. in the fluid state but not in the gel state, attributed to increased chain fluidity with the temperature both the tail melting point [67]. Layers of approximately 9 nm of LPS-Ra on mica have been reported by Tong et al.[31] using AFM to study the adsorption behaviour of LPS-Ra liposomes on mica in a buffer (25 mM KCl, 5 mM HEPES, pH 7.4). They attributed the formation of the 9 nm LPS-Ra surface layer to the rupture and spreading of the liposomes on the surface. In addition, AFM imaging also revealed areas of the surface covered with double-bilayers. Such bi-lamellar LPS-Ra aggregates of 8-9 nm in thickness have also been visualised using cryo-electron microscopy[56]. The observed structural transformation at 40 ^{o}C is also relevant to understanding the functionality of bacterial outer membranes and their interactions with antimicrobial agents. For instance, Parachini et al.[68] observed that thermally induced gel-to-liquid crystalline phase transition in the asymmetric LPS-DPPC bilayers affected the penetration by Polymyxin B, an antibiotic used for resistant Gram-negative infections.

Lu et al.[27] and Tong et al.[31] found an LPS-Ra surface layer on mica even in the absence of calcium cations. The very high ionic strength in the HEPE buffer used by Lu et al.[27] might have sufficiently suppressed the repulsion between LPS-Ra and mica. Tong et al.[31] used “a force as small as possible” to obtain their images, and indeed, they demonstrated that it was possible to squeeze out the LPS-Ra layer by applying a higher force. Our SFA results indicate the formation of a surface layer even in water, which was however weakly adsorbed to mica, readily squeezed out. In contrast, our SFA and AFM imaging results indicate that Ca^{2+} significantly enhanced the adsorption

of LPS-Ra vesicles and also the binding of the LPS-Ra bilayer to mica, which was retained even at the highest load applied. This is due to the bridging effect mediated by Ca^{2+} between the anionic groups in the LPS core and lipid A, and between the LPS core and the negatively charge mica[30]. Furthermore, a significant increase in the zeta potential of LPS-Ra in solution from -56.7 mV in pure water to -16.4 mV in 2.5 mM $CaCl_2$ solution at RT points to the reduced electrostatic repulsion between LPS-Ra and the negatively charged mica substrate.

Concluding remarks

LPS-Ra, a mutant bacterial lipopolysaccharide comprising lipid A and inner and outer cores (i.e. without the O-antigen group), represents a model molecule to study self-assembly properties of bacterial LPS in solution and at interfaces. These properties are critically important to understanding the septic effects of LPS and the structural integrity of Gram-negative bacterial membranes in which LPS is a major structural and functional component – which can be targeted in novel antimicrobial strategies. Here, the interactions between the surface layers of LPS-Ra on mica have been studied using a surface force apparatus (SFA) in pure water and 2.5 mM $CaCl_2$ (close to the physiological Ca^{2+} concentration), at RT (21 ^{o}C) and at 40 ^{o}C (above the melting temperature of the LPS-Ra acyl chains). Complementary dynamic light scattering (DLS) measurements indicated that LPS-Ra aggregates formed at RT, with the aggregate hydrodynamic diameter increasing from d_h ~ 28 in pure water to d_h ~ 80 nm as the $CaCl_2$ concentration was increased to 10 mM. The corresponding zeta potential

ζ data indicated binding of Ca^{2+} to LPS-Ra, causing ζ value to become less negative, changing from ~ -85 mV to ~-15 mV. AFM imaging revealed little adsorption of LPS-Ra aggregates on mica in pure water, but significant adsorption of a layer of spherical/ellipsoidal aggregates on mica in $CaCl_2$. The length of an LPS-Ra molecule is 4.4 nm; we thus suggest that vesicles/liposomes of LPS-Ra were formed in aqueous media.

The corresponding SFA force profiles were consistent with the adsorption behaviour of the LPS-Ra as observed from AFM imaging. That is, at 21 ^{o}C the LPS-Ra aggregates were readily squeezed out between surfaces in pure water, whereas a hard wall repulsion at surface separation D_0 = 30-40 nm in 2.5 mM Ca^{2+} indicate the strong LPS adsorption of either a monolayer of flattened LPS-Ra aggregates on each surface or ~4 LPS-Ra bilayers trapped between the surfaces. The role of Ca^{2+} of surface structuring of LPS-Ra vesicles is significant and twofold. First, Ca^{2+} bridges the negatively charged phosphate groups between LPS-Ra molecules, which stabilises the LPS-Ra vesicles against rupture at the surface. Secondly, Ca^{2+} similarly bridges between negatively charged LPS-Ra outer core and negatively charged mica, facilitating the strong adsorption of the LPS-Ra aggregates, also observed with AFM. Considering that many biological surfaces are slightly negatively charged, this observation has implications to the mechanism of LPS sepsis.

At 40 ^{o}C ($T > T_m$), the fluidity of the LPS-Ra acyl tails was greatly enhanced, manifesting in multilayer steps in the surface force profiles as the surface aggregate layers were compressed, due to LPS-Ra bilayers being squeezed out in a process

similar to membrane fusion. Such layering behaviours also confirm bilayers as a structural feature in LPS-Ra aggregates, thus substantiating our suggestion that LPS-Ra vesicles formed in aqueous media, consistent with the DLS hydrodynamic diameter d_h data. These unprecedented SFA results provide insights on the stability and structural integrity of LPS-Ra membranes – how it could be challenged and tuned by the presence of Ca^{2+} and modest temperature changes. Although the chain-melting effect has been induced by temperature elevation in this study, one could envisage alternative routes to impart similar effects, e.g. by inserting nano-objects of certain size and surface chemistry into the membrane to induce structural disorders[69-72].

LPS-Ra shares many structural and chemical features with other rough LPS mutants and smooth bacterial LPS. The well-defined differences between these mutants would provide a framework in which the roles of different structural features (e.g. the inner core, outer core, and O-antigen) can be studied systematically , and the effect of solution conditions (such as the temperature, ionic strength, pH, and the presence of nanoparticles and antimicrobial proteins) on the structure of the LPS membranes can be studied using quantitative and rigorous physicochemical techniques, such as the Israelachvili surface force apparatus (SFA).

Acknowledgements

W.H.B. would like to acknowledge funding from the EPSRC (EP/H034862/1 and Building Global Engagement in Research (BGER)), European Cooperation in Science and Technology (CMST COST) Action CM1101 “Colloidal Aspects of Nanoscience for

Innovative Processes and Materials", and Marie Curie Initial Training Network (MCITN) on "Soft, Small, and Smart: Design, Assembly, and Dynamics of Novel Nanoparticles for Novel Industrial Applications" (NanoS3, Grant no. 290251). C.R. was supported by an Everett Scholarship at the University of Bristol. Dr Georgia Pilkington (now at the Royal Institute of Technology, Stockholm) is acknowledged for her significant contributions to setting up the SFA measurement system and darkroom in Bristol, and Dr Tim Snow (now at Diamond Light Source, UK) is acknowledged for writing the SFA interfacing software – both are co-authors on the forthcoming manuscripts. We acknowledge support from the Bristol University Alumni Association for C.R. in attending the 27th European Colloids and Interface Society conference 2017. Dr Luisa Islas and Dr Robert Harniman are thanked for their help with AFM imaging. W.H.B. would also like to thank Dr Boyan Bonev (University of Nottingham) for a helpful discussion on binding of Ca^{2+} to LPS.

Dedication

We dedicate this paper to the memory of Jacob Israelachvili, a pioneering and inspiring scientist in the measurement and understanding of surface forces.

References

1. *Antimicrobial resistance: global report on surveillance*. World Health Organization (WHO): 2014.
2. Hawkey, P. M., The growing burden of antimicrobial resistance. *Journal of Antimicrobial Chemotherapy* **2008,** *62*, I1-I9.
3. Tripathy, A.; Sen, P.; Su, B.; Briscoe, W. H., Natural and bioinspired nanostructured bactericidal surfaces. *Adv Colloid Interfac* **2017,** *248*, 85-104.
4. Silhavy, T. J.; Kahne, D.; Walker, S., The Bacterial Cell Envelope. *Cold Spring Harbor Perspectives in Biology* **2010,** *2* (5).
5. Salton, M. R. J., Structure and function of bacterial cell membranes. *Annual Review of Microbiology* **1967,** *21*, 417-442.
6. von Bodman, S. B.; Willey, J. A.; Diggle, S. P., Cell-cell communication in bacteria: United we stand. *Journal of Bacteriology* **2008,** *190* (13), 4377-4391.
7. Cockburn, J. J. B.; Abrescia, N. G. A.; Grimes, J. M.; Sutton, G. C.; Diprose, J. M.; Benevides, J. M.; Thomas, G. J.; Bamford, J. K. H.; Bamford, D. H.; Stuart, D. I., Membrane structure and interactions with protein and DNA in bacteriophage PRD1. *Nature* **2004,** *432* (7013), 122-125.
8. Raetz, C. R. H., Biochemistry of Endotoxins. *Annual Review of Biochemistry* **1990,** *59*, 129-170.
9. Clifton, L. A.; Skoda, M. W. A.; Le Brun, A. P.; Ciesielski, F.; Kuzmenko, I.; Holt, S. A.; Lakey, J. H., Effect of Divalent Cation Removal on the Structure of Gram-Negative Bacterial Outer Membrane Models. *Langmuir* **2015,** *31* (1), 404-412.
10. Seydel, U.; Koch, M. H. J.; Brandenburg, K., Structural Polymorphisms of Rough Mutant Lipopolysaccharides Rd to Ra from Salmonella minnesota. *Journal of Structural Biology* **1993,** *110* (3), 232-243.
11. Poltorak, A.; He, X. L.; Smirnova, I.; Liu, M. Y.; Van Huffel, C.; Du, X.; Birdwell, D.; Alejos, E.; Silva, M.; Galanos, C.; Freudenberg, M.; Ricciardi-Castagnoli, P.; Layton, B.; Beutler, B., Defective LPS signaling in C3H/HeJ and C57BL/10ScCr mice: Mutations in Tlr4 gene. *Science* **1998,** *282* (5396), 2085-2088.
12. Mueller, M.; Lindner, B.; Kusumoto, S.; Fukase, K.; Schromm, A. B.; Seydel, U., Aggregates Are the Biologically Active Units of Endotoxin. *Journal of Biological Chemistry* **2004,** *279* (25), 26307-26313.
13. Nguyen, L. T.; Haney, E. F.; Vogel, H. J., The expanding scope of antimicrobial peptide structures and their modes of action. *Trends in Biotechnology* **2011,** *29* (9), 464-472.
14. Shai, Y., Mode of action of membrane active antimicrobial peptides. *Biopolymers* **2002,** *66* (4), 236-248.
15. Zasloff, M., Antimicrobial peptides of multicellular organisms. *Nature* **2002,** *415* (6870), 389-395.
16. Rotem, S.; Raz, N.; Kashi, Y.; Mor, A., Bacterial Capture by Peptide-Mimetic Oligoacyllysine Surfaces. *Applied and Environmental Microbiology* **2010,** *76* (10), 3301-3307.
17. Sandetskaya, N.; Engelmann, B.; Brandenburg, K.; Kuhlmeier, D., Application of immobilized synthetic anti-lipopolysaccharide peptides for the isolation and detection of bacteria. *European Journal of Clinical Microbiology & Infectious Diseases* **2015,** *34* (8), 1639-1645.
18. Nilsson, A.; Fant, C.; Nyden, M.; Holmberg, K., Lipopolysaccharide removal by a peptide-functionalized surface. *Colloids and Surfaces B-Biointerfaces* **2005,** *40* (2), 99-106.
19. Uppu, D. S. S. M.; Haldar, J., Lipopolysaccharide Neutralization by Cationic-Amphiphilic Polymers through Pseudoaggregate Formation. *Biomacromolecules* **2016,** *17* (3), 862-873.
20. Domingues, M. M.; Castanho, M.; Santos, N. C., rBPI(21) Promotes Lipopolysaccharide Aggregation and Exerts Its Antimicrobial Effects by (Hemi)fusion of PG-Containing Membranes. *Plos One* **2009,** *4* (12).
21. Domingues, M. M.; Inacio, R. G.; Raimundo, J. M.; Martins, M.; Castanho, M.; Santos, N. C., Biophysical characterization of polymyxin b interaction with LPS aggregates and membrane model systems. *Biopolymers* **2012,** *98* (4), 338-344.

22. Holst, O. M. A. P. B., P. J. , Overview of the glycosylated components of the bacterial cell envelope. In *Microbial Glycobiology: Structures, Relevance and Applications*, 1st ed.; Holst, O. B., P. J. ; von Itzstein, M., Ed. Elsevier: London, 2009; pp 1-13.
23. Abuillan, W.; Schneck, E.; Korner, A.; Brandenburg, K.; Gutsmann, T.; Gill, T.; Vorobiev, A.; Konovalov, O.; Tanaka, M., Physical interactions of fish protamine and antisepsis peptide drugs with bacterial membranes revealed by combination of specular x-ray reflectivity and grazing-incidence x-ray fluorescence. *Physical Review E* **2013,** *88* (1).
24. Schneck, E.; Schubert, T.; Konovalov, O. V.; Quinn, B. E.; Gutsmann, T.; Brandenburg, K.; Oliveira, R. G.; Pink, D. A.; Tanaka, M., Quantitative determination of ion distributions in bacterial lipopolysaccharide membranes by grazing-incidence X-ray fluorescence. *Proceedings of the National Academy of Sciences of the United States of America* **2010,** *107* (20), 9147-9151.
25. Jeworrek, C.; Evers, F.; Howe, J.; Brandenburg, K.; Tolan, M.; Winter, R., Effects of Specific versus Nonspecific Ionic Interactions on the Structure and Lateral Organization of Lipopolysaccharides. *Biophysical Journal* **2011,** *100* (9), 2169-2177.
26. Schneck, E.; Papp-Szabo, E.; Quinn, B. E.; Konovalov, O. V.; Beveridge, T. J.; Pink, D. A.; Tanaka, M., Calcium ions induce collapse of charged O-side chains of lipopolysaccharides from Pseudomonas aeruginosa. *Journal of the Royal Society Interface* **2009,** *6*, S671-S678.
27. Lu, Q. Y.; Wang, J.; Faghihnejad, A.; Zeng, H. B.; Liu, Y., Understanding the molecular interactions of lipopolysaccharides during E. coli initial adhesion with a surface forces apparatus. *Soft Matter* **2011,** *7* (19), 9366-9379.
28. Clifton, L. A.; Ciesielski, F.; Skoda, M. W. A.; Paracini, N.; Holt, S. A.; Lakey, J. H., The Effect of Lipopolysaccharide Core Oligosaccharide Size on the Electrostatic Binding of Antimicrobial Proteins to Models of the Gram Negative Bacterial Outer Membrane. *Langmuir* **2016,** *32* (14), 3485-3494.
29. Snyder, S.; Kim, D.; McIntosh, T. J., Lipopolysaccharide bilayer structure: Effect of chemotype, core mutations, divalent cations, and temperature. *Biochemistry* **1999,** *38* (33), 10758-10767.
30. Kaufmann, S.; Ilg, K.; Mashaghi, A.; Textor, M.; Priem, B.; Aebi, M.; Reimhult, E., Supported Lipopolysaccharide Bilayers. *Langmuir* **2012,** *28* (33), 12199-12208.
31. Tong, J.; McIntosh, T. J., Structure of Supported Bilayers Composed of Lipopolysaccharides and Bacterial Phospholipids: Raft Formation and Implications for Bacterial Resistance. *Biophysical Journal* **2004,** *86* (6), 3759-3771.
32. Vagenende, V.; Ching, T. J.; Chua, R. J.; Jiang, Q. Z.; Gagnon, P., Self-assembly of lipopolysaccharide layers on allantoin crystals. *Colloids and Surfaces B-Biointerfaces* **2014,** *120*, 8-14.
33. Wang, Q.; Zhang, J. P.; Smith, T. R.; Hurst, W. E.; Sulpizio, T., An electrokinetic study on a synthetic adsorbent of crystalline calcium silicate hydrate and its mechanism of endotoxin removal. *Colloids and Surfaces B-Biointerfaces* **2005,** *44* (2-3), 110-116.
34. Parikh, S. J.; Chorover, J., ATR-FTIR study of lipopolysaccharides at mineral surfaces. *Colloids and Surfaces B-Biointerfaces* **2008,** *62* (2), 188-198.
35. Jucker, B. A.; Harms, H.; Zehnder, A. J. B., Polymer interactions between five gram-negative bacteria and glass investigated using LPS micelles and vesicles as model systems. *Colloids and Surfaces B-Biointerfaces* **1998,** *11* (1-2), 33-45.
36. Oliveira, R. G.; Schneck, E.; Quinn, B. E.; Konovalov, O. V.; Brandenburg, K.; Gutsmann, T.; Gill, T.; Hanna, C. B.; Pink, D. A.; Tanaka, M., Crucial roles of charged saccharide moieties in survival of gram negative bacteria against protamine revealed by combination of grazing incidence x-ray structural characterizations and Monte Carlo simulations. *Physical Review E* **2010,** *81* (4).
37. Kotra, L. P.; Golemi, D.; Amro, N. A.; Liu, G. Y.; Mobashery, S., Dynamics of the lipopolysaccharide assembly on the surface of Escherichia coli. *Journal of the American Chemical Society* **1999,** *121* (38), 8707-8711.

38. Lam, N. H.; Ma, Z.; Ha, B. Y., Electrostatic modification of the lipopolysaccharide layer: competing effects of divalent cations and polycationic or polyanionic molecules. *Soft Matter* **2014,** *10* (38), 7528-7544.
39. Nascimento, A.; Pontes, F. J. S.; Lins, R. D.; Soares, T. A., Hydration, ionic valence and cross-linking propensities of cations determine the stability of lipopolysaccharide (LPS) membranes. *Chemical Communications* **2014,** *50* (2), 231-233.
40. Obst, S.; Kastowsky, M.; Bradaczek, H., Molecular dynamics simulations of six different fully hydrated monomeric conformers of Escherichia coli re-lipopolysaccharide in the presence and absence of Ca2+. *Biophysical Journal* **1997,** *72* (3), 1031-1046.
41. Herrmann, M.; Schneck, E.; Gutsmann, T.; Brandenburg, K.; Tanaka, M., Bacterial lipopolysaccharides form physically cross-linked, two-dimensional gels in the presence of divalent cations. *Soft Matter* **2015,** *11* (30), 6037-6044.
42. Garidel, P.; Blume, A., 1,2-Dimyristoyl-sn-glycero-3-phosphoglycerol (DMPG) monolayers: influence of temperature, pH, ionic strength and binding of alkaline earth cations. *Chemistry and Physics of Lipids* **2005,** *138* (1–2), 50-59.
43. Simoni, S. F.; Bosma, T. N. P.; Harms, H.; Zehnder, A. J. B., Bivalent cations increase both the subpopulation of adhering bacteria and their adhesion efficiency in sand columns. *Environmental Science & Technology* **2000,** *34* (6), 1011-1017.
44. Seydel, U.; Brandenburg, K.; Koch, M. H. J.; Rietschel, E. T., Supramolecular structure of lipopolysaccharide and free lipid-A under physiological conditions as determined by synchrotron small-angle X-ray diffraction. *European Journal of Biochemistry* **1989,** *186* (1-2), 325-332.
45. Briscoe, W. H.; Titmuss, S.; Tiberg, F.; Thomas, R. K.; McGillivray, D. J.; Klein, J., Boundary lubrication under water. *Nature* **2006,** *444* (7116), 191-194.
46. Israelachvili, J. N.; Tabor, D., The Measurement of Van Der Waals Dispersion Forces in the Range 1.5 to 130 nm. *Proceedings of the Royal Society of London. A. Mathematical and Physical Sciences* **1972,** *331* (1584), 19.
47. Delgado, A. V.; Gonzalez-Caballero, E.; Hunter, R. J.; Koopal, L. K.; Lyklema, J., Measurement and interpretation of electrokinetic phenomena - (IUPAC technical report). *Pure Appl Chem* **2005,** *77* (10), 1753-1805.
48. Ohshima, H., *Theory of Colloid and Interfacial Electric Phenomena*. Academic Press: London, 2006.
49. Klein, J.; Perahia, D.; Warburg, S., Forces between polymer-bearing surfaces undergoing shear. *Nature* **1991,** *352* (6331), 143-145.
50. Kienle, D. F.; Kuhl, T. L., Analyzing Refractive Index Profiles of Confined Fluids by Interferometry. *Analytical Chemistry* **2014,** *86* (23), 11860-11867.
51. Bergstrand, A.; Svanberg, C.; Langton, M.; Nydén, M., Aggregation behavior and size of lipopolysaccharide from Escherichia coli O55:B5. *Colloids and Surfaces B: Biointerfaces* **2006,** *53* (1), 9-14.
52. Aurell, C. A.; Hawley, M. E.; Wistrom, A. O., Direct Visualization of Gram-Negative Bacterial Lipopolysaccharide Self-Assembly. *Molecular Cell Biology Research Communications* **1999,** *2*, 42-46.
53. Aurell, C. A.; Wistrom, A. O., Critical Aggregation Concentrations of Gram-Negative Bacterial Lipopolysaccharides (LPS). *Biochemical and Biophysical Research Communications* **1998,** *253* (1), 119-123.
54. Santos, N. C.; Silva, A. C.; Castanho, M. A. R. B.; Martins-Silva, J.; Saldanha, C., Evaluation of Lipopolysaccharide Aggregation by Light Scattering Spectroscopy. *ChemBioChem* **2003,** *4* (1), 96-100.
55. Andrä, J.; Koch, M. H. J.; Bartels, R.; Brandenburg, K., Biophysical Characterization of Endotoxin Inactivation by NK-2, an Antimicrobial Peptide Derived from Mammalian NK-Lysin. *Antimicrobial Agents and Chemotherapy* **2004,** *48* (5), 1593-1599.
56. Richter, W.; Vogel, V.; Howe, J.; Steiniger, F.; Brauser, A.; Koch, M. H.; Roessle, M.; Gutsmann, T.; Garidel, P.; Mantele, W.; Brandenburg, K., Morphology, size distribution, and

aggregate structure of lipopolysaccharide and lipid A dispersions from enterobacterial origin. *Innate Immun* **2010,** *17* (5), 427-38.
57. Bello, G.; Eriksson, J.; Terry, A.; Edwards, K.; Lawrence, M. J.; Barlow, D.; Harvey, R. D., Characterization of the Aggregates Formed by Various Bacterial Lipopolysaccharides in Solution and upon Interaction with Antimicrobial Peptides. *Langmuir* **2015,** *31* (2), 741-751.
58. Wlodek, M.; Kolasinska-Sojka, M.; Szuwarzynski, M.; Kereiche, S.; Kovacik, L.; Zhou, L. Z.; Islas, L.; Warszynski, P.; Briscoe, W. H., Supported lipid bilayers with encapsulated quantum dots (QDs) via liposome fusion: effect of QD size on bilayer formation and structure. *Nanoscale* **2018,** *10* (37), 17965-17974.
59. Garcia-Manyes, S.; Oncins, G.; Sanz, F., Effect of Temperature on the Nanomechanics of Lipid Bilayers Studied by Force Spectroscopy. *Biophysical Journal* **2005,** *89* (6), 4261-4274.
60. Inagaki, M.; Kawaura, T.; Wakashima, H.; Kato, M.; Nishikawa, S.; Kashimura, N., Different contributions of the outer and inner R-core residues of lipopolysaccharide to the recognition by spike H and G proteins of bacteriophage ϕX174. *FEMS Microbiology Letters* **2003,** *226* (2), 221.
61. Brandenburg, K.; Andrä, J.; Müller, M.; Koch, M. H. J.; Garidel, P., Physicochemical properties of bacterial glycopolymers in relation to bioactivity. *Carbohydrate Research* **2003,** *338* (23), 2477-2489.
62. Mueller, M.; Lindner, B.; Dedrick, R.; Schromm, A. B.; Seydel, U., Endotoxin: physical requirements for cell activation. *Journal of Endotoxin Research* **2005,** *11* (5), 299-303.
63. Sasaki, H.; White, S. H., Aggregation Behavior of an Ultra-Pure Lipopolysaccharide that Stimulates TLR-4 Receptors. *Biophysical Journal* **2008,** *95* (2), 986-993.
64. Lanne, A. B. M.; Goode, A.; Prattley, C.; Kumari, D.; Drasbek, M. R.; Williams, P.; Conde-Alvarez, R.; Moriyon, I.; Bonev, B. B., Molecular recognition of lipopolysaccharide by the lantibiotic nisin. *Biochim Biophys Acta Biomembr* **2019,** *1861* (1), 83-92.
65. Horn, R. G., Direct measurement of the force between two lipid bilayers and observation of their fusion. *Biochimica et Biophysica Acta (BBA) - Biomembranes* **1984,** *778* (1), 224-228.
66. Kastowsky, M.; Gutberlet, T.; Bradaczek, H., Molecular modelling of the three-dimensional structure and conformational flexibility of bacterial lipopolysaccharide. *Journal of Bacteriology* **1992,** *174* (14), 4798-4806.
67. Wong, J. Y.; Park, C. K.; Seitz, M.; Israelachvili, J., Polymer-Cushioned Bilayers. II. An Investigation of Interaction Forces and Fusion Using the Surface Forces Apparatus. *Biophysical Journal* **1999,** *77* (3), 1458-1468.
68. Paracini, N.; Clifton, L. A.; Skoda, M. W. A.; Lakey, J. H., Liquid crystalline bacterial outer membranes are critical for antibiotic susceptibility. *Proceedings of the National Academy of Sciences* **2018,** *115* (32), E7587.
69. Beddoes, C. M.; Berge, J.; Bartenstein, J. E.; Lange, K.; Smith, A. J.; Heenan, R. K.; Briscoe, W. H., Hydrophilic nanoparticles stabilising mesophase curvature at low concentration but disrupting mesophase order at higher concentrations. *Soft Matter* **2016,** *12* (28), 6049-57.
70. Beddoes, C. M.; Case, C. P.; Briscoe, W. H., Understanding nanoparticle cellular entry: A physicochemical perspective. *Adv Colloid Interface Sci* **2015,** *218*, 48-68.
71. Bulpett, J. M.; Snow, T.; Quignon, B.; Beddoes, C. M.; Tang, T. Y.; Mann, S.; Shebanova, O.; Pizzey, C. L.; Terrill, N. J.; Davis, S. A.; Briscoe, W. H., Hydrophobic nanoparticles promote lamellar to inverted hexagonal transition in phospholipid mesophases. *Soft Matter* **2015,** *11* (45), 8789-800.
72. Fox, L. J.; Richardson, R. M.; Briscoe, W. H., PAMAM dendrimer - cell membrane interactions. *Adv Colloid Interface Sci* **2018,** *257*, 1-18.